Direct-detection free-space laser transceiver test-bed

Michael A. Krainak, Jeffrey R. Chen, Philip W. Dabney, Jeffrey F. Ferrara, Wai H. Fong,
Anthony J. Martino, Jan F. McGarry, Stephen M.Merkowitz,
Caleb M. Principe, Xiaoli Sun, Thomas W. Zagwodzki
NASA Goddard Space Flight Center, Greenbelt, MD USA 20771

ABSTRACT

NASA Goddard Space Flight Center is developing a direct-detection free-space laser communications transceiver test bed. The laser transmitter is a master-oscillator power amplifier (MOPA) configuration using a 1060 nm wavelength laser-diode with a two-stage multi-watt Ytterbium fiber amplifier. Dual Mach-Zehnder electro-optic modulators provide an extinction ratio greater than 40 dB. The MOPA design delivered 10-W average power with low-duty-cycle PPM waveforms and achieved 1.7 kW peak power. We use pulse-position modulation format with a pseudo-noise code header to assist clock recovery and frame boundary identification. We are examining the use of low-density-parity-check (LDPC) codes for forward error correction. Our receiver uses an InGaAsP 1 mm diameter photocathode hybrid photomultiplier tube (HPMT) cooled with a thermo-electric cooler. The HPMT has 25% single-photon detection efficiency at 1064 nm wavelength with a dark count rate of 60,000/s at -22 degrees Celsius and a single-photon impulse response of 0.9 ns. We report on progress toward demonstrating a combined laser communications and ranging field experiment.

Keywords: Laser communications, photon counting, ytterbium fiber amplifier, hybrid photomultiplier, LDPC code

1. INTRODUCTION

Recently, an overview of NASA laser communications requirements and plans was published[1]. The most recent major NASA effort was the highly successful Mars Laser Communication Demonstration (MLCD)[2]. Unfortunately, the re-prioritization of NASA missions resulted in the cancellation of the Mars Telecommunications Orbiter (and with it the MLCD payload opportunity). To date, a free-space laser communication demonstration (a logical pathfinder for future NASA missions) has not been deployed. To assist in securing a spacecraft deployment opportunity, NASA-GSFC initiated the development of an in-house laser communications/ranging transceiver test bed.

2. SYSTEM DEMONSTRATION

2.1 Laser Communications Test-bed System Overview and Approach

We are developing a low-cost test-bed to simulate and develop photon-starved laser communications. In addition, we incorporate methods from our recent investigations[3] that use communications signal format pseudo-noise code modulation to demonstrate combined laser ranging and communications. To keep the cost low, we use off-the-shelf components wherever possible, perform our signal processing and error correction functions in (non-real-time) software and use a 10 ns receiver time-slot width. The test bed assists in component and signal processing performance tests and evaluation. Our goal is to improve the US industrial capability for future NASA space mission requirements. Numerous terrestrial fiber optic telecommunications components are available for use at 1550 nm wavelength. These systems typically operate at relatively high photon flux at the receiver to support very high data rates. In contrast, the deep-space NASA mission requirements dictate reduction of spacecraft resources. The highest possible practical receiver sensitivity then serves to balance the optimization of the transmitter aperture, laser power and pointing requirements. At present, this performance comes from a photon-counting detector based system. The lowest-cost, highest performance, photon-counting detector that meets our communications requirements at the present time is the InGaAsP photocathode hybrid photomultiplier tube (HPMT) (a.k.a. intensified photodiode - IPD) operating in the 900-1300 nm wavelength range. Fortunately, cost-competitive high-power efficient Yb fiber lasers in this wavelength range (i.e. 1060 nm) are readily available. Since Yb lasers are now widely used for laser welding - the economy of scale places high power Yb on the same level as high power Er (or Er/Yb). We believe our approach provides the highest performance per cost laboratory

demonstration for photon-starved communication links. However, additional considerations are important for selecting the operating wavelength of space-qualified systems. We have plans for a similar demonstration at 1550 nm using a smaller area (for reduced dark counts) InGaAs photocathode HPMT photon-counting detector and an Er fiber laser.

Deep-space systems for NASA applications typically trade high data rate performance against system sensitivity to reduce spacecraft resource requirements (including cost). In free-space laser communications, the use of the high alphabet pulse position modulation (PPM) format has been shown to facilitate this trade.

Figure 1 shows a System Diagram of our Laser Communications Transceiver Test Bed.

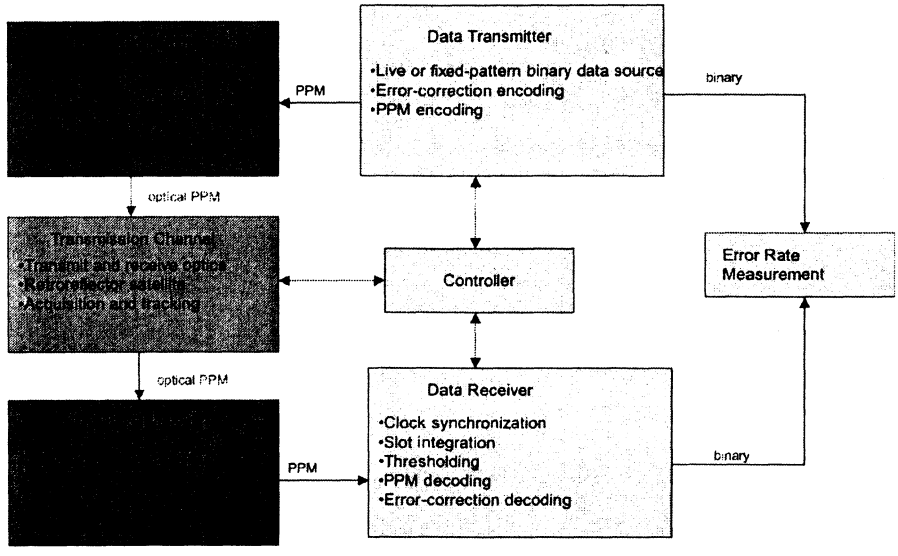

Fig. 1. Laser Communications Test-bed System Diagram

2.2 Laser Transmitter

Our transmitter design is similar to that for the 5W PPM transmitter[4,5] developed for the Mars Laser Communications Demonstration (MLCD). Our transmitter is capable of transmitting variable M-PPM waveforms with 10 W average power at 1064 nm. Based on a flexible master-oscillator, power-amplifier (MOPA) design, the transmitter is single-mode (SM) and polarization maintaining (PM). A prototype transmitter was built solely from commercial-off-the-shelf (COTS) fiber optic components, which greatly accelerated development and lowered the cost.

The transmitter supports low duty cycle 64-ary PPM modulation format with pulse slot widths of 10ns. An Ytterbium-doped fiber amplifier (YDFA) operating in saturation boosts the average signal power to 10 W with peak pulse powers exceeding 1.7kW.

Figure 2 shows the optical design diagram for the PPM transmitter. The master laser is a Fiber Bragg Grating (FBG) stabilized 1064 nm laser diode made by Lumics, operated at 80 mW output power with a narrow linewidth of 0.42GHz. A polarizing isolator protects the laser from optical feedback from the fiber amplifier.

The CW master laser output is modulated using two LiNbO3 Mach-Zehnder modulators manufactured by EOSpace. A custom built YDFA preamplifier is inserted between the two modulators to boost the signal power to greater than 10 mW to saturate the power amplifier. The second MZM after the preamp blocks the leakage between pulses. This combination achieves the high (>40 dB) extinction ratio (ER) necessary to deliver high-fidelity low-duty-cycle waveforms. The second MZM after the preamplifier gates out the amplified spontaneous emission (ASE) from the preamplifier. High ER is maintained with auto-bias control cards made by YY labs that lock the modulator DC bias at the null point. The modulators are driven with RF electrical pulses to generate the required PPM waveform. The average input to the fiber preamplifier is as low as -14 dBm (including modulation and component insertion losses). At this low

input power, a low-noise preamplifier is necessary to minimize the buildup of ASE. We choose to pump the preamplifier through the core (SM core-pumping) rather than cladding pumping to achieve efficiently high inversion hence low ASE noise in the preamplifier. The Nufern SM PM single-clad Yb fiber for the preamplifier is divided into two sections and a 4nm 1064nm filter and an isolator are inserted between them to reject ASE and to a void multi-path interference (MPI). Each Yb fiber section was core-pumped with a JDSU Inc. SM PM 976 nm laser diode though a 1064/976 nm PM wavelength division multiplexer (WDM). The first Yb fiber was co-pumped (at 240 mW) to optimize the noise figure, and the second fiber counter-pumped (at 280 mW) for higher gain. Each pump laser passes through a 976nm filter that prevents ASE and 1064 nm signal from hitting the pump diode. We chose 976 nm over 915 nm pumping wavelength because the SM PM 976 nm pump diodes are readily available and space qualified. Furthermore, the 976 nm core pumping creates an inversion high enough to minimize the ASE noise (with spontaneous emission factor n_{sp} close to the minimum = 1), yet not too high (<50%) to cause photo-darkening in the Yb fiber.

The power amplifier is a COTS 10 W single-frequency SM PM Yb double-clad fiber amplifier made by IPG Corporation, pumped by multimode laser diodes that efficiently generate high average (and peak) powers. To further reduce ASE noise and MPI, another 4 nm 1064 nm filter and isolator are inserted between the preamplifier and the power amplifiers. While the polarization extinction ratio (PER) can rapidly degrade when many PM components are concatenated, each of the three SM PM isolators also functions as a polarizer to help maintaining PER>17 dB in our system.

Although the 1064 nm seed laser diode is rated 150 mW, it is derated so the power to the first MZM is below 40 mW to avoid photorefractive damage to the MZM. In our system, the preamplifier boosts the -14 dBm input to 13 dBm, corresponding to 27 dB gain. The power amplifier further amplifies the signal to 40 dBm average (1700 W peak) power, achieving a net gain of ~54 dB for the whole amplifier train.

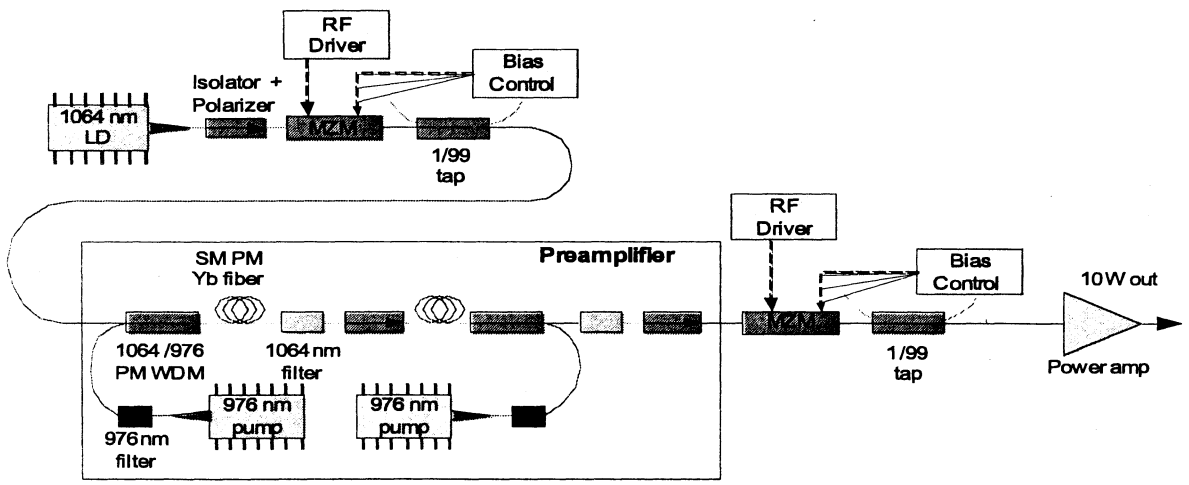

Fig. 2. Optical design of the transmitter for free space laser communication

The properties measured in the prototype transmitter operation include spectral width, on-off extinction ratio, average and peak power, and waveforms. The modulation extinction ratio at the 10 W output of the power amplifier was measured to be 47dB, more than adequate to delivery waveforms at duty cycles as low as 1/250.

While high-peak-power fiber amplifiers are desirable for photon-efficient communication, performance can be limited by spectral-broadening nonlinearities such as self-phase modulation (SPM), or stimulated Brillouin scattering (SBS), which can reduce output power through reflections and lead to destructive pulsing. At the 10 ns pulse length, SBS was

found to be significant. To reduce the level of SBS while maintaining the 10-ns pulse required by the receiver, the 10 ns slot is filled with a burst of multiple sub-pulses, as shown in Figure 3. The width of the sub pulses is 0.5 ns, and the separation between two adjacent sub-pulses is 1.1 ns (leaving 0.6 ns blank space between sub-pulses). This sub-pulse modulation broadens the laser linewidth to 1.35 GHz, (far beyond SBS bandwidth) and therefore effectively mitigates the SBS. While the reduced duty cycle of this waveform increased the peak power a factor of about 2, the short sub-pulse length more than compensated to reduce SBS to a negligible level. At 10 W average output power, the power amplifier peak power was estimated to be 1.7 kW. Since a monitor port for backward SBS is not accessible to us, we monitored the SBS onset from the power amplifier output power vs. the pump diode current, shown in Figure 4. Up to the 10 W average output power, there is no sign of SBS onset that causes roll-off of the output power. Figure 5 shows the measured input and output spectra for the power amplifier at various powers levels.

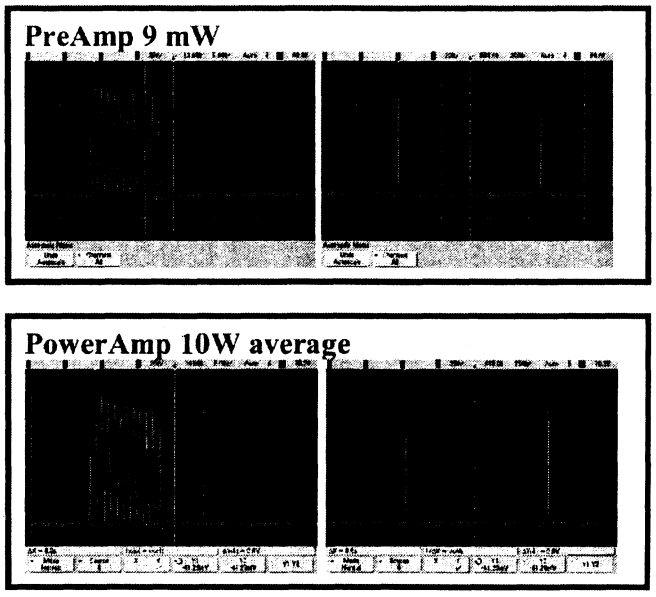

Fig. 3. Comparison of optical pre-amplifier and 10 W amplifier output waveform.

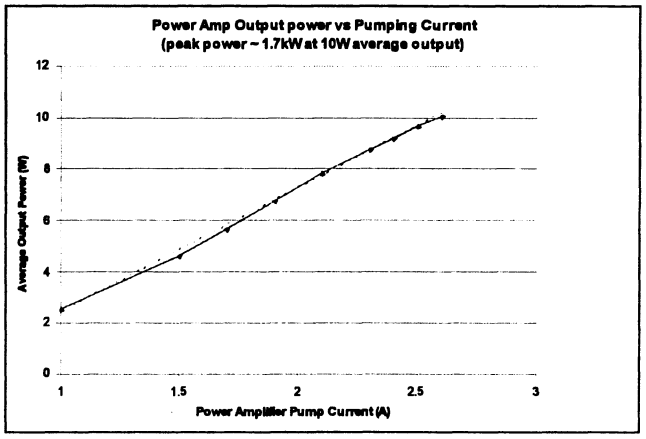

Fig. 4. Dependence of average output power on pump diode current for the power amplifier. The average optical output power is 10 W at 2.7 A because several pump diodes are connected in series.

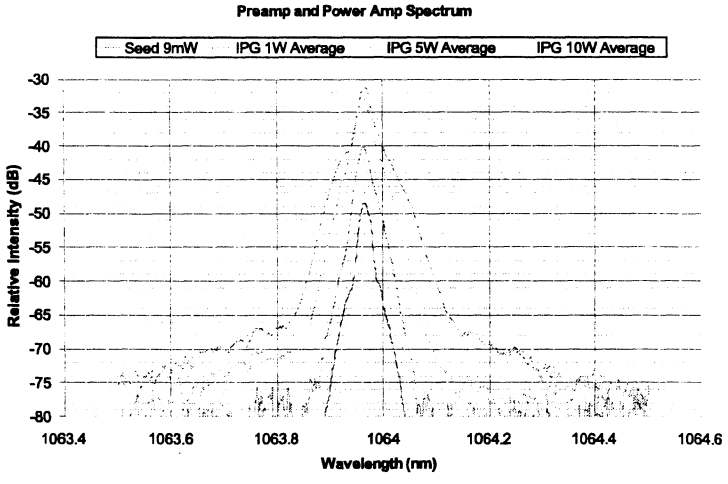

Fig. 5. Spectra of the input and output of the power amplifier

2.3 Photon counting detector

The receiver uses a transfer electron (TE) InGaAsP photocathode hybrid photomultiplier (HPMT) from Intevac Inc. It has high quantum efficiency at 950-1300 nm wavelengths, as high as 30% at 1064 nm[6]. Table 1 shows characteristics of several purchased HPMTs. Another alternative is the TE InGaAsP photomultiplier tubes (PMT), commercially available from Hamamatsu with about 9% quantum efficiency for hand-selected devices. We have packaged several HPMT into a turnkey thermal electrical cooled (TEC) housing. We also developed a low noise high voltage power supply system that significantly reduced the dark count rate. The highest photon counting efficiency achieved was 25% at 1064 nm and a dark count rate of about 50,000/s. A previous publication[7] provides details of these detectors and packaging. For the initial laboratory experiment, we used a lower quantum efficiency device with 15% photon counting efficiency and about 60,000/s dark count rate. A significant advantage, especially for large telescope atmospheric channel experiments, is the 1 mm diameter detector surface in combination with the aforementioned parameters.

Table 1. Characteristics of several purchased InGaAsP hybrid photomultiplier tubes.

Serial Number	Detection Efficiency	Dark Counts	Temperature
201	25%	60 kcps	-22 C
205	26%	60 kcps	-25 C
207	17%	110 kcps	-18 C

2.4 Data Format and Transmitter/Receiver Electronics

The transmitter electronics is responsible for encoding and formatting the data and generating the signal sent to the pulse generator which is set up to specifically match the pulse shapes required by the laser system. The data encoding and modulation is performed off-line to generate a binary data pattern. The data is uploaded to the buffer of a National Instruments PCI-6542 Digital Waveform Generator that can store up to 8Mbits binary data. It is configured to send out the stored data at the clock edges and repeat the encoded message indefinitely. Future improvements to this system will include real-time data and clock encoding, but the current system is sufficient for demonstrating the basic system performance.

The data frame used consists of a clock synchronization pattern followed by the encoded data, which includes blocks of both the information and the parity (redundancy) bits for forward error correction. The detailed format of the frame was chosen to optimize the performance of the test-bed setup and desired bit error rate.

The clock synchronization pattern is a maximum-length pseudo-noise (PN) sequence that is easily identified by the receiver via a cross correlation of the received signal with the original PN code. This allows location of the data frame boundary and clock synchronization to the transmitter. The optimal length of the sequence depends on the expected signal to noise ratio and the frequency of repetition is determined by the uncertainty in the clock drift rates and Doppler shifts due to the relative transmitter/receiver motion.

Our initial data code words consist of 2048 bits and carry a 1024 bit message. The other 1024 bits carry the redundancy information used by the forward error correction discussed below. A 64-ary pulse position modulation (PPM) is applied to each code word. After the sync pattern, twelve code words are transmitted as a block and then repeated for eight blocks before the next sync pattern. This method of repetition offers a modest amount of interleaving and increases the signal to noise by allowing the receiver to average over the eight repetitions (at the cost of a lower data rate). The size of the code words, number of code words and reputations included in a frame are variables in this experiments and are easily adjusted to handle different noise conditions at the optical site.

The receiver consists of the photon counting detector (described above) followed by a fast event counter. For this demonstration, a Model P7889 FAST ComTec Multichannel Scalar board was used as the event counter. The data from this board is recorded to disk for off-line analysis (described in the system software section below).

2.5 Error Correcting Code

The error correction code used in the test-bed is a binary linear block code where every $K = 1024$ bits of data has $M = 1024$ bits of parity (redundant information) appended producing a codeword size of $N = 2048$. The code has a coding rate of $R = K/N = 1/2$. For this demonstration, we are using a low-density parity check (LDPC) code.

2.5.1 LDPC Background

Discovered by Gallager[8] in 1962 but mostly ignored until its rediscovery[9,10] in 1996, LDPC codes[11] are not error correction codes in the traditional sense, i.e. Reed-Solomon, Hamming etc.. Instead, they can be any linear block code that works well with the decoder. In essence, LDPC codes are defined by the decoding and not by any particular code or mapping. They are typically specified by a very sparse, i.e. very small number of 1s compared to the number of 0s in a parity check matrix $\boldsymbol{H}$ of dimension M x N. Shown to achieve error performance very near the Shannon limit (channel capacity), LDPC codes power lies in a decoding algorithm called the sum product algorithm (SPA). This algorithm iteratively updates the channel log-likelihood ratio (LLR) by passing messages between two types of processors. A full iteration is a complete cycle of messages sent back and forth between the two node processor types.

The processors are known as node types because the SPA can be visually depicted as a bi-partite graph called a Tanner graph[12] with N "variable nodes" vertices and $M = N - K$ "constraint nodes" vertices. The interconnections (called edges) of the graph are defined by every "1" element of parity check matrix of the code and are the means by which messages travel between nodes. Connecting multiple edges to each node forms a set or grouping. This allows all nodes to operate in a distributed localized manner producing inherent parallel processors. The messages for a particular edge are numerical values based on extrinsic information (i.e. message values other than it's own) that the nodes update (once per iteration) according to mathematical rules. There are two different rules, one for each node type. The SPA defines the variable node rule as a simple sum of extrinsic messages connected to a variable node. However, the constraint node rule is more complex (i.e. the hyperbolic arc tangent of the product of the hyperbolic tangent of every extrinsic message connected to a constraint node). Less complex variants to the SPA replace the complex constraint rule with an approximate rule. For example, in the Min-Sum algorithm, the constraint rule is: minimize all extrinsic messages connected to the constraint node. The penalty for this approximation is a fraction of a dB of power efficiency for a given error performance in AWGN channels. Other variants lie between the SPA and Min-Sum in complexity and performance.

2.5.2 LDPC Characteristics and Issues

LDPC codes can be easy to create but difficult to optimize. Error floors can exist at low bit error rates, which limit the error correcting power of the code. Fortunately, there has been some success with techniques to lower the LDPC code error floor. Whereas error floor eradication is not practical with other code types. There appears to be a complexity tradeoff between LDPC codes that approach the channel capacity and the required number of iterations. Codes that try to minimize the power gap between the code BER performance and channel capacity require more iterations. However, there is a point of diminishing returns, where no further gains in error performance occur beyond a certain number of

iterations. For many LDPC codes, 50 iterations is a typical point simulation maximum. Unfortunately, analytical tools to predict iterative performance of the SPA are currently not available. By using a stopping rule in the simulations, statistical data can be collected to determine the average number of iterations for a particular LDPC code. This figure can help determine the maximum or a fixed number of iterations for a particular hardware implementation. To a point, the higher above the average the number of iterations is set, the better the error performance will be. More important, the LDPC code must have an iterative performance that complies with the data rate requirement.

Almost a universal issue with LDPC codes is that of encoding at the transmitter. Since LDPC codes are designed via the parity check matrix, the generator matrix is usually a secondary consideration. Traditional methods of Gaussian elimination can lead to generator matrices of high density of 1's and large complexity. Quasi-cyclic codes are codes that have the ***H*** matrix constructed by using circulants (square matrices where each row or column is an end around shift of the previous row or column) as sub-matrices. Quasi-cyclic[13] LDPC codes have good error performance and simple encoding complexity under certain conditions.

2.5.3 LDPC Code Definition

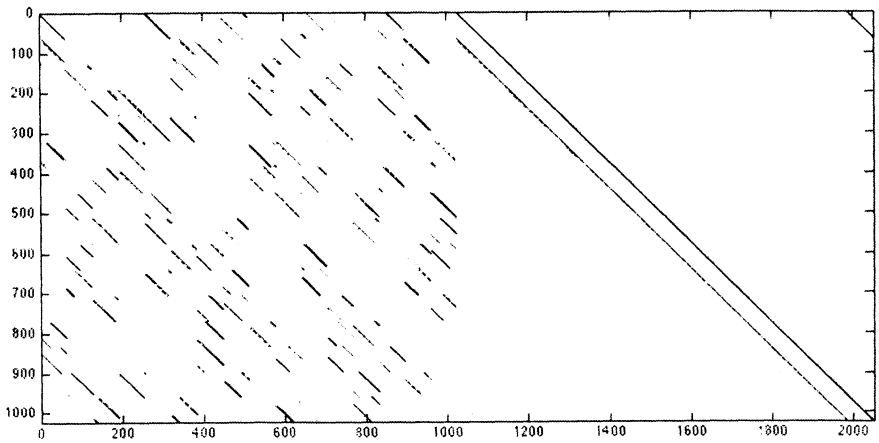

Fig. 6. LDPC S-IRA (2048,1024) ***H*** matrix scatter plot

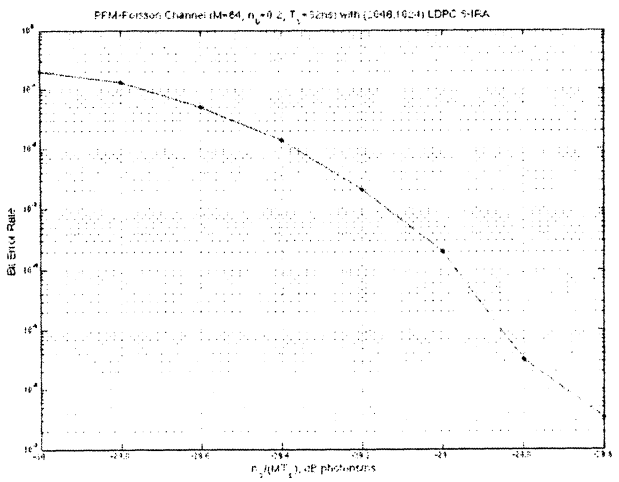

Fig. 7. LDPC S-IRA PPM-Poisson Channel Performance

Figure 6 shows a scatter plot of the $\boldsymbol{H}$ matrix for the test bed. This type of code is called a Structured-Irregular Repeat Accumulate code (S-IRA). This is a quasi-cyclic code using size 64 (64 x 64 matrices) circulants. The column weights (total number of 1's) have two values: weight 5 for columns 0 to 1023 and weight 2 for columns 1024 to 2047. The circulants are of right shifts (i.e. rows are a right shift from it's previous row) and have column weights of 1 which are called permutation circulants in the literature. To encode in a quasi-cyclic manner, a permutation of one column of circulants of weight 5 to one column of weight 2 is required in order to invert the right 1024 x 1024 sub-matrix. As a side note, by removing a "1" from position (0, 2047) of the $\boldsymbol{H}$ matrix, an Irregular Repeat Accumulate code (IRA) can be formed. This variant of the original S-IRA code has the characteristic that the $\boldsymbol{H}$ matrix can be used to encode the data by backward substitution. Both codes have similar error performance[14].

Simulations shown in Figure 7 show the LDPC code performance for the PPM-Poisson channel. The channel capacity is around -30.7 dB photons/ns for an M=64, PPM-Poisson Channel with expected dark photon count n_b= 0.2 and a slot time T_s =32ns. The performance is around 1.9 dB from capacity at 10^{-5} BER. A longer code word length, optimizing the LDPC code for the PPM-Poisson channel and combining the demodulation /decoding algorithms are methods to improve the performance.

Although serially concatenated PPM (SCPPM) turbo coding schemes[15] have shown good BER performance, we chose LDPC codes for the NASA-GSFC test bed for a number of reasons. Most notable is the inherent parallel processing of the SPA algorithm, which can provide > 4 Gbps data rates throughput[16] while turbo coding is typically limited to serial processing as result of trellis decoders. Since one major advantage of laser communications over Radio Frequency communications is high data rate (> 1 Gbps) operation without spectral allocation concerns, LDPC decoder processing speed may make it preferable for high data rate laser communications.

2.5.4 Decoding Subsystem Description

Figure 8 shows the basic architecture of the test-bed decoding subsystem. The receiver provides the channel photon counts and then the LLR/bit slicer converts the photon counts to bit-LLR values. For the laser communications channel based on photon counting, each Pulse-Position Modulation (PPM) channel symbol is determined by the received photon count within a time slot. This received symbol information is converted to bit-LLR values through a mathematical operation. Conceptually, the LLR conversion compares the received photon count to an expected photon count when the laser is on and when the laser is off, conditioned on the reception of a particular symbol. The statistics of the laser communication of the photon arrivals is Poisson and therefore the LLR calculation takes the ratio of conditional Poison probability distribution with expected number of photons arrivals equal to the expected laser photon arrival plus dark photons at the detector to the expected dark photon rate. This operation is performed for all time slots, then a bit slicing occurs where the LLR values are converted into bit-by-bit LLR values according to the bit to symbol mapping. After which, the bit-LLR values are passed to the variable nodes to prime the iterative decoding process.

The variable nodes apply their rule and pass the messages to through the network of edges, which can be looked upon as a permutation of the messages to the constraint nodes. After the application of the constraint rule, the messages are updated and sent back to the variable nodes through the permutation network. This completes one full cycle. The process will repeat or iterate until a stopping rule is reached such as a predetermined fixed number of iterations has been processed or an early out condition has occurred. A final step is to output a hard decision for the received code word. In other words, extract bit information from messages. This is accomplished by summing all messages that connected to every variable and taking only the sign information to determine the corresponding bit value. That is a negative sign can represent a "1" value and a positive sign can represent a "0". In addition, the opposite can be true; this is dependent on the encoding convention. In software, an early out condition can be defined. For example, after an iteration a legitimate code word is found, or else iterate. If no legitimate code word is found after a maximum number of iterations, stop decoding and output the last hard decision.

In linear block coding theory, an N-tuple binary code word $\boldsymbol{x}$ will lie in the null space of $\boldsymbol{H}$, that is: $\boldsymbol{Hx} = \boldsymbol{0}$, where $\boldsymbol{0}$ represents an all zeros vector of length M. This equation is used to determine if the decoded code word is legitimate. If $\boldsymbol{Hx} \neq \boldsymbol{0}$, $\boldsymbol{x}$ cannot be a code word. This is called a syndrome check and can be used as a stopping rule for the decoder and as a flag from the decoder to indicate that the received code word is not decodable.

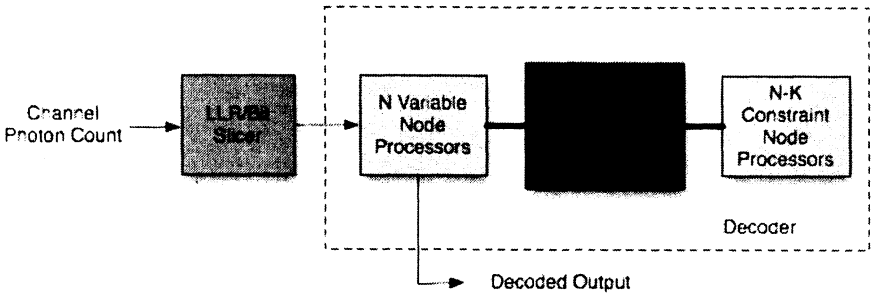

Fig. 8. Decoding Subsystem Block Diagram

2.6 System software

A full end-to-end simulation of the transmitter and receiver was developed in MATLAB. This simulation was used to test the encoding and decoding algorithms as well as clock recovery and other receiver functions in addition to predicting the performance of the system. The decoder modules can be used to analyze both real and simulated data files. A second decoder application was also independently developed in C with the intention that it be ported to operate on a real-time FPGA based system.

As shown in Figure 9, the functions performed on the transmit side are as follows. A binary data source steam is chunked into 1024-bit data blocks. These data blocks are encoded using a Low Density Parity Check (LDPC) algorithm into 2048-bit code words (this is a forward error correcting code). The stream of code words is then chunked into Pulse Position Modulation (PPM) words, which are in turn grouped into sub-frames. The PPM alphabet size and the sub-frame size are variables for this experiment. Each sub-frame is repeated "N" times, where N is another experimental variable. The sub-frames are grouped into frames. The frames are converted to PPM symbols. The frames, once converted to PPM symbol format are then pre-pended with the PN code synchronization pattern.

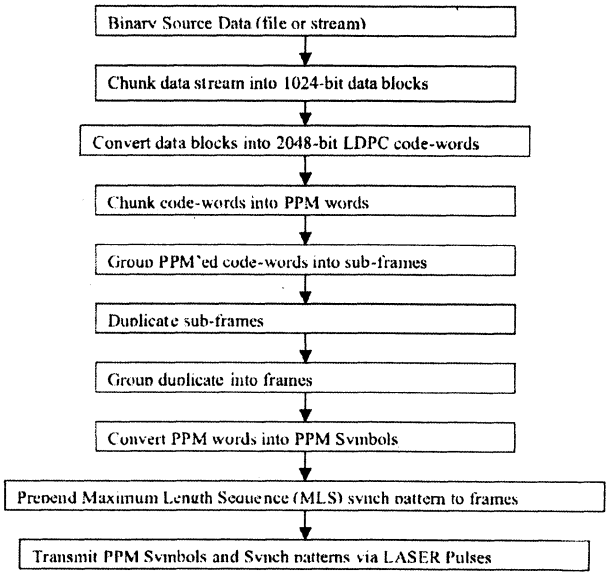

Fig. 9. Transmitter Software Functional Diagram

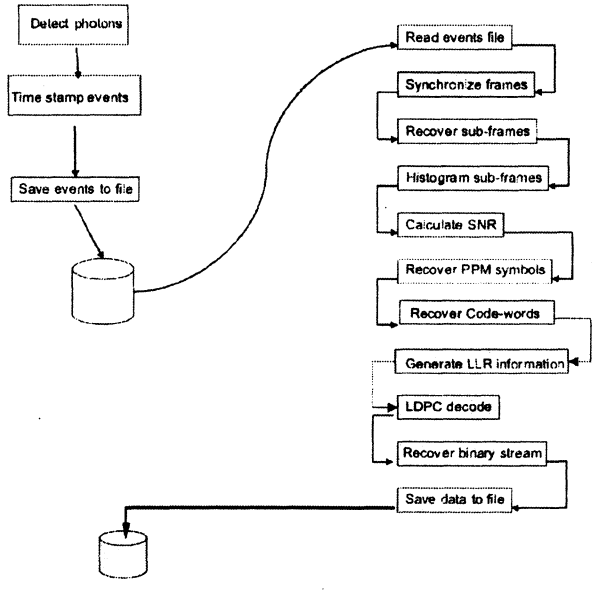

Fig. 10. Receiver Software Functional Diagram

As shown in Figure 10, the receive portion of the system begins with the detection of counts at the receiver. As events are detected they are given time-stamps that reflect the time elapsed from the start of the experiment. This information is saved to an "events file" that is subsequently read by the receive software. The software detects the frame synchronization patterns and determines the start of each frame. The sub-frames are then extracted and the duplicative data in each of the sub-frames is accumulated to create a histogram that represents the number of counts received in each PPM symbol slot. The PPM symbols and LDPC code words are recovered. The Signal-To-Noise Ratio (SNR) is determined from the counts in each slot of the received frame. The recovered code words (still in PPM symbol format) and SNR are then used in a Log-Likelihood Ratio (LLR) calculation to determine the probability that a given bit of the code word is either a one or a zero. The LLR values for each bit of each code word are then decoded using the LDPC code algorithm. The resulting binary stream of error-corrected data is then stored on a hard-drive of the receiver system.

2.7 Test bed communications performance

We achieved a preliminary communication performance of ~3 photons/bit with LDPC error correction and <ns/nb> = 0.25 (i.e. average signal counts/background counts) for a bit error rate less than 10^{-6} from our laboratory bench laser communication transceiver test-bed.

3. NEAR-TERM PLANS

3.1 Laser communication demonstration between two ground stations via satellites

We plan to conduct a combined laser communication and coded ranging demonstration by transmitting the signal from one ground station to a near earth orbit satellite and detecting the reflected signal at another ground station. A number of low earth orbit satellites carry corner cube arrays. The corner cubes (retro)reflect the laser light for satellite laser ranging (SLR) purposes. We plan to use these SLR satellites as relay stations in our free space laser communication demonstrations. The signal losses via the corner cube arrays are comparable to those in interplanetary laser communications. The effect of the earth atmosphere and the Doppler effect from the satellite motion are similar to those between earth and a spacecraft near another planet. The two stations we are going to use are the 1.2-meter telescope facility and a prototype next generation (NGSLR) system located at the Goddard Geophysical and Astronomical Observatory (GGAO) in Beltsville, Maryland. The NGSLR station has a 0.4 m telescope. Both stations are capable tracking low and high altitude satellites 20 degrees above the horizon and each satellite pass lasts about 20 minutes, depending on the satellites. They are normally used as stand alone SLR stations. The two stations are sufficiently close (~200 m) to allow each station to see the retro reflected laser light from the other station when the satellite motion and

consequently velocity aberration of the retro reflected light is along the tracking path. Shown in Figure 11 are both SLR facilities conducting nighttime laser tracking operations utilizing 532nm wavelength lasers.

3.2 Goddard Geophysical and Astronomical Observatory (GGAO) and satellite laser ranging

The NGSLR system will serve as the transmitting station for the communication demonstration. This system utilizes a 0.4 m off-axis telescope with an elevation over azithum gimbal tracking mount[17]. All telescope and gimbal mirror coatings are protected silver with a reflectivity of about 98% per surface at the communication wavelength. In normal tracking operations the Nd:YAG laser (doubled to 532nm) operates at a 2.0 kHz rate. Return pulses are detected with a quadrant micro channel plate photomultiplier (MCP-PMT). Satellite predictions are generally accurate enough to open loop point (although closed loop tracking information provided by the quadrant detector can be used to close loop track). The pointing and tracking capabilities of the telescope and mount are about 1 to 2 arc seconds. Insertion of the 1064nm communication laser is accomplished by dropping into the beam path (collimated space) a harmonic separator held in a magnetic/kinematic mount. With this beam splitter in place the outgoing 1064 nm beam can be co-bore sighted with the 532 nm SLR wavelength using our standard alignment fixtures and procedures. Additional table space at the NGSLR facility has been added to accommodate the 1064 nm laser and coupling optics. Fiber optic links between the transmitter and receiver facilities (~200 meters apart) will be in place to synchronize timing and other communication signals.

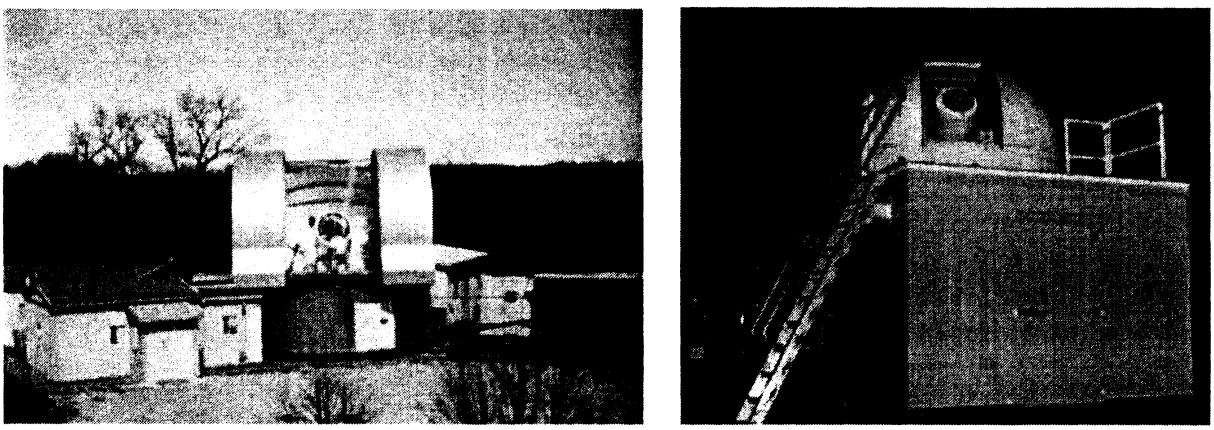

Fig. 11. NASA 1.2m Telescope Facility (left) and the 0.4m NGSLR system.

The 1.2m telescope facility will serve as the receiving station for the communication link. This system is an elevation over azimuth mount with a Coude' focus in the experimenters area on the ground floor. One Coude' room port is dedicated to the laser communication demonstration. All mirrors in the Coude' path and telescope (except the primary) have recently been coated with protected silver. The primary mirror has an enhanced aluminum coating. System receive efficiency was recently improved to ~ 80%. System pointing and tracking capabilities are at the 1 to 2 arc second level. The 532 nm tracking wavelength will be separated from the 1064 nm communication wavelength with a harmonic beam splitter[18]. Closed loop tracking on the 532 nm signal with a quadrant PMT will assure lock for the communication link. This technique of transmitting from one SLR station and receiving at another has been demonstrated multiple times between the MOBLAS-7 (transmit) and the 1.2m Facility and NGSLR (receive). The cube corner equipped satellites of interest for this demonstration include most low Earth orbit satellites (LEOs) up to LAGEOS range (6000 Km altitude). The combination of satellite altitude and cube corner cross section will determine the difficulty of the communication link.

3.3 Satellite retro-reflector link

The signal propagation losses from the retro reflected laser light increase as the fourth power of the satellite distance and is similar to those in the direct line of sight interplanetary laser communication systems. The signal amplitude will also vary over a wide dynamic range due to atmosphere turbulences and telescope pointing jitters. We estimate a link (via the NGSLR telescope, the satellite retro-reflector and the 1.2m telescope) loss of ~ 10^{13} from the laser transmitter output to

the detector surface in clear, low turbulence, night sky operation. That is, a 10 W transmitter optical output will result in 1 pW at the receiver optical detector surface.

ACKNOWLEDGMENTS

This work was supported by the NASA GSFC Director's Reserve, NASA-GSFC IRAD, the NASA-HQ Space Communications and Navigation (SCaN), and the NASA Earth Science Technology Organization (ESTO) laser ranging programs. We would like to thank: Shadi AbuSurra, William E. Ryan, Yifei Zhang of U. of Arizona and David Fisher of GSFC/MEI.

REFERENCES

[1] H. Memmati, "Interplanetary laser communications," Optics & Photonics News, 18(11), pp. 22-27 (2007)
[2] D.M. Boroson, Chen Chien-Chung, B. Edwards, "Overview of the Mars laser communications demonstration project" IEEE LEOS Digest of the Summer Topical Meetings 25-27 pp. 5 - 7 (2005)
[3] X. Sun, J. B. Abshire, M. A. Krainak, and W. B. Hasselbrack, "Photon counting pseudorandom noise code laser altimeters," Proc. SPIE 6771 (2007)
[4] N.W. Spellmeyer, D.O. Caplan, and M.L. Stevens, "Design for a 5-Watt PPM Transmitter for the Mars Laser Communications Demonstration," LEOS Summer Topical Meetings, pp. 51-52 (2005)
[5] N. W. Spellmeyer, et al, "A High-Efficiency Ytterbium-Doped Fiber Amplifier Designed for Interplanetary Laser Communications", Optical Fiber Communication and the National Fiber Optic (2007)
[6] W. Farr, "Ground based photon counting detection for the 2010 Mars Laser Communications Demonstration" 4th International Conference on New Developments in Photon Detection Beaune, France (2005)
[7] X. Sun, M. A. Krainak, W. B. Hasselbrack, and R. A. La Rue, "Photon counting performance measurements of transfer electron InGaAsP photocathode hybrid photomultiplier tubes at 1064 nm wavelength" Proc. SPIE 6583 (2007)
[8] R. G. Gallager, "Low density parity check codes," IRE Trans. Inform. Theory, **IT-8**, pp. 21-28 (1962)
[9] D. J. C. MacKay and R. M. Neal, "Near Shannon limit performance of low density parity check codes," Electro. Lett., **32**, pp. 1645-1646 (1996)
[10] N. Wiberg, "Code and Decoding on General Graphs," Ph.D. Diss., Dept. of Electrical Engineering, University of Linkoping, Sweden (1996)
[11] W. E. Ryan, "An Introduction to LDPC Codes," in CRC Handbook for Coding and Signal Processing for Recording Systems (B. Vasic, ed.) CRC Press (2004)
[12] R. M. Tanner, "A Recursive Approach to Low Complexity Codes," IEEE Trans. Inform. Theory, **27** pp. 533-547 (1981)
[13] Z. Li, L. Chen, L. Zeng, S. Lin, and W. Fong, "Efficient Encoding of Quasi-Cyclic Low Density Parity Check Codes," IEEE Transactions on Communications, **54**(1), pp. 71-81 (2006)
[14] Y. Zhang, "Design of Low-Floor Quasi-Cyclic IRA Codes and Their FPGA Decoders," Ph.D. Diss., Dept. of Electrical and Computer Engineering, University of Arizona, USA (2007)
[15] B. Moision, J. Hamkins, M. Cheng, "Design of a Coded Modulation for Deep Space Optical Communications," UCSD 1st Workshop on Information Theory and Applications (2006)
[16] K.K. Gunnam, G.S. Choi, M.B. Yeary, "A Parallel VLSI Architecture for Layered Decoding for Array LDPC Codes" IEEE 20th International Conference on VLSI Design (VLSI Design, 2007), pp. 738 – 743, (2007)
[17] T. W. Zagwodzki, J. F. McGarry, J. J. Degnan, and T. Varghese "Two-color SLR experiments at the GSFC 1.2-m telescope," Proc. SPIE 3218, 113 (1997)
[18] J. J. Degnan "Engineering progress on the fully automated photon-counting SLR2000 satellite laser ranging station," Proc. SPIE 3865, 76 (1999).